

3-D-printed X/Ku-band High-gain Integrated Lens MIMO Antenna Using CPW-fed Magnetolectric dipoles

Aditya Singh*, Carlos E. Saavedra

Department of Electrical and Computer Engineering, Queen’s University, Kingston, Ontario, Canada, K7L 3N6.
e-mail: singh.aditya@queensu.ca, saavedra@queensu.ca

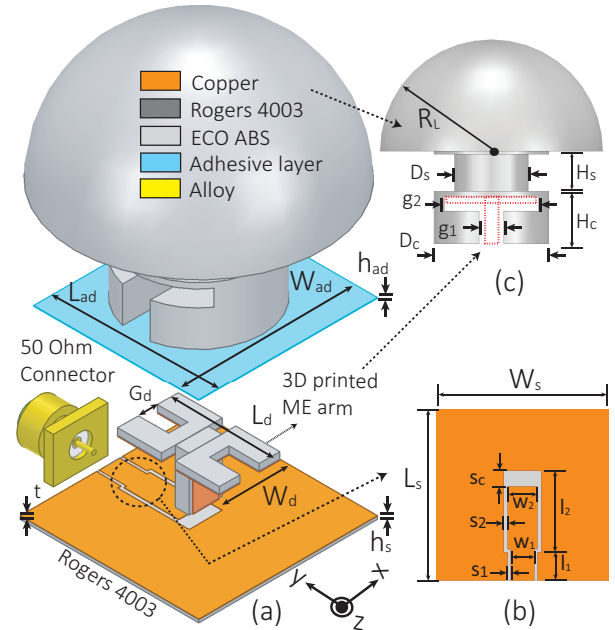
Abstract

A four-element high-gain multiple-input multiple-output (MIMO) antenna array covering X and Ku bands is presented that utilizes three-dimensional (3-D)-printed integrated lens antenna (ILA) as the MIMO element. The ILA uses a dielectric-embedded magnetolectric (ME) dipole as the radiating element to obtain antenna miniaturization and wide impedance bandwidth (IBW). Full-wave simulations exhibits a total active reflection coefficient, $|TARC|$ and $|S_{11}| \leq -10$ dB, for 75% bandwidth while minimum isolation is above 25 dB. The peak gain is ~ 10.9 dBi while the envelope correlation coefficient (ECC) is ≤ 0.003 . The measured element prototype exhibits IBW of 75% and maximum measured realized gain of 10.7 dBi wherein the footprint at lowest operating wavelength is $0.69\lambda^2$.

1 Introduction

Three-dimensional (3-D) printing technology has spurred significant interest owing to its capability to provide high-precision fabrication for antennas, dielectric lenses, and more. Thus, 3-D printing technology is highly conducive for integrated lens antenna (ILA), since it can greatly benefit from modern high-precision 3-D printer technology [1]. ILA may use a variety of radiating components including electric dipoles such as a dual bow-tie antenna [3], helical antenna [2], patch antennas [4] et cetera. Moreover, magnetolectric (ME) dipoles are attractive choice for wideband applications as they offer wide bandwidth, symmetrical and wide beam radiation in E and H plane with high gain. Some ILAs with ME dipoles as lens feed has been proposed for millimeter wave MIMO using Luneburg lens [5]. In addition, the multiple-input multiple-output technology has been widely adopted and a variety of antennas in sub-6 GHz [6], X-band [7, 8], Ku-band [9] as well as fifth-generation millimeter-wave bands [10] have been proposed.

This paper presents a 3-D-printed integrated Lens antenna element with an embedded magnetolectric dipole and its four-element MIMO array. A 3-D-printed cylindrical dielectric structure is used to house the ME dipole, wherein it miniaturizes the antenna. The ME dipole itself uses a 3-D-printed arm and has parallel stripline and coplanar-



var.	L_s	W_s	L_d	W_d	G_d	R_L	D_c	D_s	L_{ad}	W_{ad}	-	-
val.	31.2	31.2	17.76	14.4	6	21.6	22.3	14.4	28.8	31.2	-	-
var.	s_1	s_2	s_c	l_1	l_2	h_s	h_{ad}	g_1	g_2	w_1	w_2	t
val.	0.45	0.6	2.4	12.5	0.5	0.142	2.88	4.8	0.2	3.6	4.6	0.035

Figure 1. Integrated lens antenna with ME dipole embedded in a cylindrical dielectric structure (a) Exploded view (b) Cross-sectional view showing PS to dipole connection. All the design parameters are tabulated (unit: mm).

waveguide feeds that aids to obtain lens integration with dielectric 3-D printing as well as wide impedance bandwidth, high gain with good MIMO metrics.

2 MIMO Element

2.1 Antenna design

Fig. 1 (a) shows the exploded view of the integrated lens antenna (ILA) wherein the radiating component is the magnetolectric (ME) dipole embedded in the cylindrical dielectric structure. The material used for 3-D printing the hemispherical lens and the cylindrical structure is ECO ABS.

The relative permittivity is around 2.3 while the loss tangent is below 0.05 over the frequency range of interest. The measured electrical properties as characterized in [11] has been used in the full-wave HFSS simulations. The loss tangent value is assumed to be 0.015 [12] to be conservative with the radiation efficiency simulations. The conductivity of the connector alloy is considered to be same as copper. The ME dipole is realized by coating a thin layer of copper on the 3-D-printed ME arm as shown in Fig. 1 (a). This can be achieved by using an adhesive copper tape on the 3-D-printed arm enabling it to work as ME dipole with parallel-stripline (PS) feed (metal strips on both sides of the vertical arm separated by dielectric material). This PS line interfaces with the antenna feed system. The feed comprises of a coplanar waveguide (CPW) designed on a 0.5 mm thick Rogers-4003 substrate ($\epsilon_r = 3.55$, $\tan \delta = 0.0027$). A 50 Ω edge mounted SMA connector is utilized. The details of the CPW feed are shown in Fig. 1 (b), the width of the signal trace of the CPW towards the PS line side is w_2 which is reduced to w_1 at connector side to avoid shorting. The corresponding slot gap of the CPW line is s_2 and s_1 respectively. Finally, the line is terminated in an open circuit with slot width as s_c that interfaces with the PS line.

The typical electrical size for wideband ME dipoles ($IBW \geq 70\%$) is larger than $0.5\lambda \times 0.5\lambda$ where λ is the free space wavelength at lowest operating frequency. However, for wideband multiple-input multiple-output (MIMO) systems, adopting such elements may result in large sizes. To reduce the element size, the electrical resonances of the ME antennas can be shifted to lower frequencies by embedding the ME dipole in a dielectric material. Herein, we employ cylindrical ECO ABS structure of height H_c to embed the antenna. To attach the 3-D-printed cylinder to the substrate, the ARSeal double sided adhesive tape is utilized. Furthermore, to allow for the easy assembly of the antenna, slots are provided that can be easily achieved with 3-D printing. Thus, only with dielectric filament, fused deposition modeling (FDM) method, and copper tape, the proposed integrated lens antenna can be fabricated. Consequently, the size of the ME dipole reduces, it may also introduce dielectric resonance of the cylindrical structure to improve the antenna performance as observed in [13] albeit with liquid dielectric. Finally, to enhance the gain of the antenna, a hemispherical lens of radius R_L is added on top of the embedded ME dipole as shown in Fig. 1 (c). As seen, the lens is placed at a distance H_s from the cylindrical structure. All the design parameters are tabulated in Fig. 1. The fabricated prototype is shown in Fig. 2 wherein the lens and ME dipole arm are 3D printed while copper tape is used to realize conductive part of ME dipole.

2.2 Reflection and Far-field Characteristics

Fig. 3 depicts the variation of $|S_{11}|$ with frequency, wherein the simulated -10 dB impedance bandwidth (IBW) is 75%. As seen, the measured and simulated responses correspond well, except that the former is shifted downwards and the

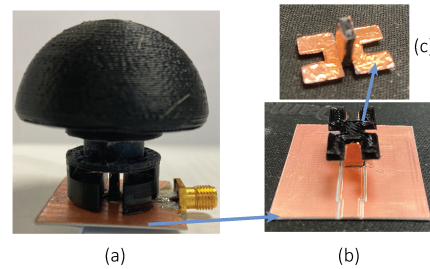


Figure 2. Fabricated prototype (a) final , (b) without lens, (c) ME dipole 3-D printed arm with copper tape.

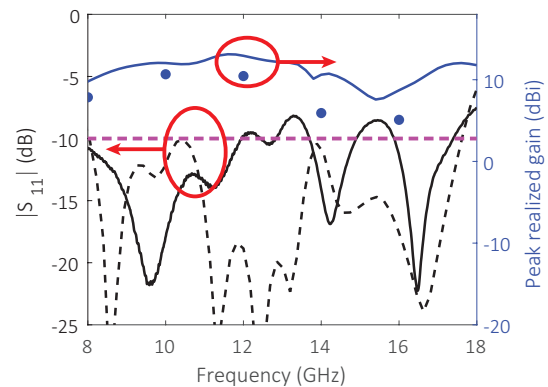


Figure 3. Simulated and measured $|S_{11}|$ and peak realized gain for the proposed antenna depicted in Fig. 1. Solid black line and solid marker show measured values.

impedance match is deteriorated at some points. The difference may be attributed to the fabrication tolerances. The peak realized gain and radiation pattern of the prototype is measured in the anechoic chamber and reported in Fig. 3 and Fig. 4. In both xz and yz planes, the cross-polarized components are below 20 dB, where xz plane shows higher cross-polarized radiation mainly attributed to the CPW-PS feed [14]. As seen from Fig. 4, the simulated and measured patterns agree well to each other. The measured realized gains are lower than the simulated ones, indicating that in the simulations the loss tangent considered for ECO ABS is lower than actual value.

3 Four-element MIMO Antenna

Fig. 5 depicts the proposed MIMO antenna with all the design parameters tabulated. The MIMO array comprises of four elements with center-to-center inter-element distance of L_e and arranged such that adjacent ME dipoles are oriented orthogonal to each other. Consequently, it improves the MIMO response since it allows for lower mutual coupling among elements [6]. Moreover, when different ports are excited, it provides diversity in the radiation pattern, since the relative position and orientation varies for each el-

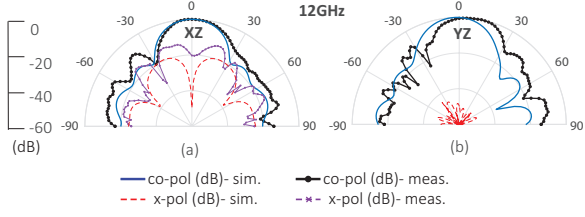


Figure 4. Normalized simulated and measured radiation pattern of the element at 12 GHz in the XZ and YZ planes.

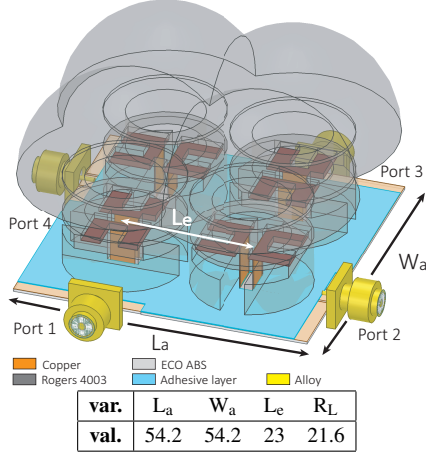


Figure 5. Four-element MIMO antenna employing center-to-center inter-element distance of L_e and antenna size $L_a \times W_a$. The rest of antenna parameters same as tabulated in Fig. 1. (unit: mm)

ement. To evaluate the performance of the MIMO antenna, one port is excited at a time while terminating the rest of the ports with 50Ω .

3.1 Reflection and Isolation Characteristics

Fig. 6 depicts the simulated reflection coefficient and isolation when port 1 excitation is considered. The simulated -10 dB impedance bandwidth (IBW) is 75%, whereas the isolation is better than 25 dB over the operating band. Owing to the symmetry, the results for other port excitation are similar, hence, omitted for brevity.

3.2 Far Field and MIMO Response

The simulated radiation patterns in xz and yz plane are depicted in Fig. 8. Patterns are presented for the case when element 1 is excited and rest of ports are terminated with 50Ω . Herein, the patterns remain nearly similar to the element albeit the peak realized gain, as seen from Fig. 7 reduces due to proximity of other ILAs. The total active reflection coefficient (TARC) is presented in Fig. 7, which evaluates the effect of mutual coupling and random signal combina-

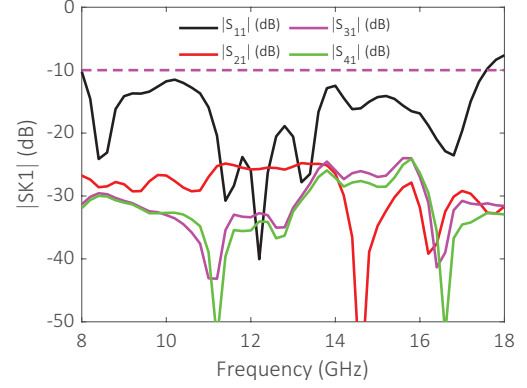


Figure 6. Simulated reflection coefficient and isolation curves ($|S_{K1}|$ ($K = 1$ and 3)) when element 1 is excited and rest of ports are terminated to 50Ω .

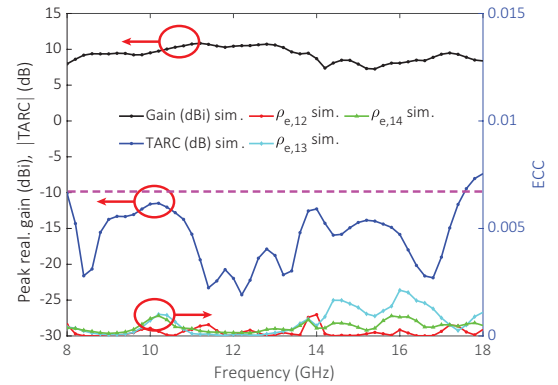


Figure 7. Simulated peak realized gain, $|TARC|$, and envelope correlation coefficient (ECC) trends when port 1 is excited while the rest of ports are terminated to 50Ω .

tions among elements in MIMO antennas, is defined as [15]

$$TARC (dB) = 10 \log \frac{\sum_{n=1}^4 |b_n|^2}{\sum_{i=1}^4 |a_i|^2} \quad (1)$$

where a_n and b_n are incident and reflected signals at the n^{th} port. Herein, $|TARC| \leq -10$ dB is achieved over the complete operating band. Furthermore, the simulated envelope correlation coefficient (ECC) is calculated from simulated far fields in HFSS, where, $\rho_{e,ij}$ represents the ECC between the i^{th} and j^{th} ports. As seen in Fig. 7, the ECC (ρ_e) remains remarkably low, thus obtaining good MIMO performance for the proposed antenna.

Conclusion

A wideband and high-gain four-element multiple-input multiple-output (MIMO) antenna that utilizes 3-D-printed magnetoelectric (ME) dipole-fed integrated lens antenna as

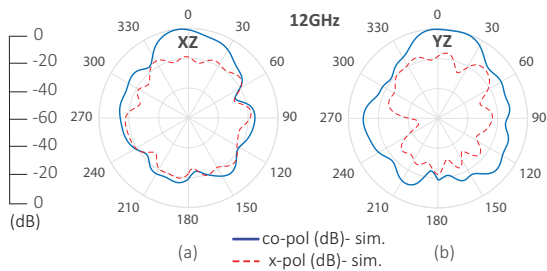


Figure 8. Normalized simulated radiation pattern of the four-element MIMO antenna at 12 GHz in the XZ and YZ planes, when element 1 is excited and rest of ports are terminated with 50Ω .

its element has been proposed. Measured element demonstrated an impedance bandwidth (IBW) of 75% and maximum realized gain of 10.7 dBi. The MIMO metrics presented indicate good MIMO performance with 75% IBW and maximum realized gain of 10.5 dBi for X/Ku band. The antenna can be particularly useful for applications that allow higher antenna profile and require high-gain with MIMO operation. The gain, size and bandwidth performance can be further improved by adopting different in-fill density for lens, reducing the air gap for the embedded ME dipole by utilizing fully 3-D-printed designs that enable simultaneous conductive and dielectric printing.

Acknowledgements

This work was supported, in part, by the Natural Sciences and Engineering Research Council of Canada (NSERC) Discovery Grant RGPIN-2022-05204.

References

- [1] E.-S. Jo and D. Kim, "3-d printer based lens design method for integrated lens antennas," *IEEE Antennas and Wireless Propagation Letters*, vol. 17, no. 11, pp. 2090–2093, 2018.
- [2] M. F. Farooqui and A. Shamim, "3-d inkjet-printed helical antenna with integrated lens," *IEEE Antennas and Wireless Propagation Letters*, vol. 16, pp. 800–803, 2017.
- [3] G. H. Lee, S. Kumar, H. C. Choi, and K. W. Kim, "Wideband high-gain double-sided dielectric lens integrated with a dual-bowtie antenna," *IEEE Antennas and Wireless Propagation Letters*, vol. 20, no. 3, pp. 293–297, 2021.
- [4] N. T. Nguyen, A. V. Boriskin, L. Le Coq, and R. Sauleau, "Improvement of the scanning performance of the extended hemispherical integrated lens antenna using a double lens focusing system," *IEEE Transactions on Antennas and Propagation*, vol. 64, no. 8, pp. 3698–3702, 2016.
- [5] Y. Li, L. Ge, M. Chen, Z. Zhang, Z. Li, and J. Wang, "Multibeam 3-d-printed luneburg lens fed by magnetolectric dipole antennas for millimeter-wave mimo applications," *IEEE Transactions on Antennas and Propagation*, vol. 67, no. 5, pp. 2923–2933, 2019.
- [6] A. Singh and C. E. Saavedra, "Fluidically reconfigurable mimo antenna with pattern diversity for sub-6-ghz 5g relay node applications," *Canadian Journal of Electrical and Computer Engineering*, vol. 43, no. 2, pp. 92–99, 2020.
- [7] D. Sharma, R. Kumar, and R. K. Vishwakarma, "Multi-standard planar compact 4-port mimo with enhanced performance for ism/5g nr/c/wlan/x band applications," *Optik*, vol. 269, p. 169871, 2022.
- [8] B. Feng, J. Lai, Q. Zeng, and K. L. Chung, "A dual-wideband and high gain magneto-electric dipole antenna and its 3d mimo system with metasurface for 5g/wimax/wlan/x-band applications," *IEEE Access*, vol. 6, pp. 33 387–33 398, 2018.
- [9] A. Desai, C. D. Bui, J. Patel, T. Upadhyaya, G. Byun, and T. K. Nguyen, "Compact wideband four element optically transparent mimo antenna for mm-wave 5g applications," *IEEE Access*, vol. 8, pp. 194 206–194 217, 2020.
- [10] M. T. Hussain, M. S. Sharawi, S. Podilchack, and Y. M. M. Antar, "Closely packed millimeter-wave mimo antenna arrays with dielectric resonator elements," in *2016 10th European Conference on Antennas and Propagation (EuCAP)*, 2016, pp. 1–4.
- [11] H. Banting and C. E. Saavedra, "Dielectric spectroscopy of fluids and polymers for microwave microfluidic circuits and antennas," *IEEE Transactions on Microwave Theory and Techniques*, vol. 69, no. 1, pp. 337–343, 2021.
- [12] P. I. Deffenbaugh, R. C. Rumpf, and K. H. Church, "Broadband microwave frequency characterization of 3-d printed materials," *IEEE Transactions on Components, Packaging and Manufacturing Technology*, vol. 3, no. 12, pp. 2147–2155, 2013.
- [13] C. Song, E. L. Bennett, J. Xiao, and Y. Huang, "Multi-mode hybrid antennas using liquid dielectric resonator and magneto-electric dipole," *IEEE Transactions on Antennas and Propagation*, vol. 69, no. 6, pp. 3132–3143, 2021.
- [14] A. Singh and C. E. Saavedra, "Low-profile cpw-ps-fed magnetolectric antenna," *IEEE Antennas and Wireless Propagation Letters*, vol. 20, no. 12, pp. 2471–2475, 2021.
- [15] M. S. Sharawi, "Printed multi-band mimo antenna systems and their performance metrics [wireless corner]," *IEEE Antennas and Propagation Magazine*, vol. 55, no. 5, pp. 218–232, 2013.